

A Reliable Context-Aware and Temporal Planning Framework for Autonomous Driving

Argho Dey, Yunfei Yin, *Member, IEEE*, Swachha Ray, Md Minhazul Islam, Zheng Yuan, Sijing Xiong, Hongyu Liu, and Zhiqiu Huang

Abstract—Safe operation of autonomous vehicles in dense urban traffic depends on perception and planning that remain reliable when onboard sensing is degraded. In real driving conditions, camera observations are frequently corrupted by occlusion, motion blur, illumination change, and sensor noise, and when such degraded observations are aggregated indiscriminately over time, trajectory planning becomes unstable and collision risk rises for both the ego vehicle and surrounding road users. Recent Bird's-Eye-View (BEV) approaches unify perception and planning through a shared spatial representation, but most fuse temporal information across frames without assessing the reliability of the underlying observations. We present a Reliable Context-Aware and Temporal Planning framework for Autonomous Driving (RCT-AD) that explicitly models feature quality and temporal consistency to support safer, more consistent planning. A Reliable Context Awareness module scores per-frame reliability and selectively retains trustworthy features through a quality-gated First-In-Last-Out (FILO) memory mechanism, reconstructing degraded observations from reliable historical context so that corrupted inputs do not destabilize the scene representation. A Temporal Trajectory Planner captures long-term dependencies and multi-agent interactions to produce smoother, safety-aware trajectories, while a joint detection-and-segmentation head injects semantic and motion cues into the shared BEV space to strengthen scene understanding. Experiments on the nuScenes autonomous driving benchmark show that RCT-AD improves perception accuracy, motion prediction, and planning robustness over recent end-to-end baselines, achieving 61.5 nuScenes Detection Score, 52.9 mean Average Precision, and 52.3 mean Intersection over Union, while maintaining competitive computational efficiency suitable for real-time deployment.

Index Terms—Autonomous driving, Bird's-Eye-View perception, temporal memory, semantic reasoning, trajectory planning, multi-task learning.

I. INTRODUCTION

AUTONOMOUS driving has emerged as a transformative area of artificial intelligence [2], aiming to equip vehicles with human-like perception, contextual understanding, and decision-making abilities for safe navigation in complex real-world environments. With the rapid

progress of deep learning and multi-sensor perception technologies, modern autonomous vehicles have achieved remarkable improvements in environmental understanding and motion planning. Nevertheless, most existing autonomous driving systems still follow a modular pipeline that separates perception [13], prediction [24], [30] and planning [4], [10] into independent components. Although this modular design improves interpretability and allows each component to be optimized individually, it also disrupts the continuous flow of information across the pipeline. As a consequence, errors introduced during early perception stages can propagate to later modules, often resulting in degraded performance in dynamic and uncertain driving environments [17], [18]. Recent research has explored unified end-to-end autonomous driving frameworks that jointly model perception and planning within a single architecture. Approaches such as BridgeAD [7] attempt to bridge the gap between perception and decision-making by learning shared representations across tasks. However, existing end-to-end methods still face several challenges in real-world environments. Many approaches rely on detection-oriented Bird's-Eye-View (BEV) representations combined with simple spatial-temporal aggregation strategies [11], [15], [16], [23], where observations from different frames are treated equally without considering their reliability. In practice, camera-based perception is often affected by occlusions, motion blur, illumination changes, and sensor noise, which may introduce corrupted features into temporal representations. When these unreliable observations are aggregated indiscriminately, they can destabilize BEV representations and negatively influence downstream perception and planning performance.

In addition, many existing frameworks lack sufficient semantic supervision and robust temporal modeling. Detection-focused BEV representations often fail to capture important contextual cues such as drivable areas, lane topology, and interaction dynamics, which are essential for safe and interpretable planning. Furthermore, current temporal modeling strategies usually rely on short-range feature aggregation, limiting the ability to capture long-term dependencies and multi-agent interactions.

This paragraph of the first footnote will contain the date on which you submitted your paper for review, which is populated by IEEE. This work was supported in part by the National Natural Science Foundation of China under Grant 62262045, in part by the Fundamental Research Funds for the Central Universities under Grant 2023CDJYGRH-YB11, and in part by the Open Funding of SUGON Industrial Control and Security Center under Grant CUIT-SICSC-2025-03. (*Corresponding author: Yunfei Yin*).

Argho Dey, Yunfei Yin, Swachha Ray, Md Minhazul Islam, Zheng Yuan, Sijing Xiong, Hongyu Liu, and Zhiqiu Huang are with the College of Computer Science, Chongqing University, Chongqing 400044, China (email: arghodey@stu.cqu.edu.cn; yinyunfei@cqu.edu.cn; swachharay@stu.cqu.edu.cn; mishaown@stu.cqu.edu.cn; yuanzheng@cqu.edu.cn; 202414021016t@stu.cqu.edu.cn; 202514131048T@stu.cqu.edu.cn; 202514131200@stu.cqu.edu.cn).

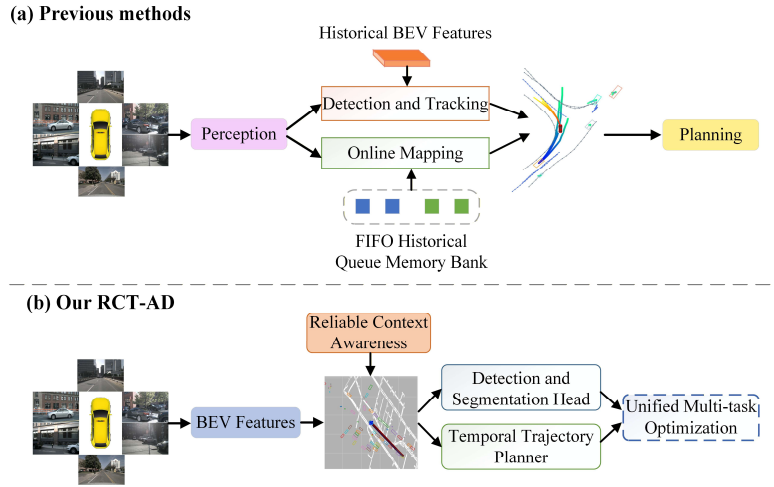


Fig. 1. Conceptual comparison between conventional end-to-end autonomous driving frameworks and the proposed RCT-AD. (a) Previous approaches aggregate temporal BEV features without evaluating observation reliability, allowing both reliable and corrupted inputs to influence motion planning, which can degrade robustness under occlusion, motion blur, or noisy visual conditions. (b) The proposed RCT-AD introduces a reliability-aware mechanism that filters unreliable observations and reconstructs degraded features using short-term reliable contextual information. This reliability-guided feature routing produces more stable BEV representations and enables consistent perception and planning outputs.

To address these issues, we propose RCT-AD, a Reliable Context-Aware Temporal Autonomous Driving framework that integrates perception, semantic reasoning, and motion planning within a unified BEV representation. The framework introduces a reliability-aware mechanism to evaluate BEV feature quality across frames and selectively preserve trustworthy contextual information through memory-guided routing. By combining reliability-aware perception, semantic supervision, and temporal interaction modeling, RCT-AD provides a more stable and interpretable end-to-end autonomous driving system.

Our main contributions are as follows:

1. **Reliable Context Awareness (RCA):** We propose a reliability-aware feature routing module that evaluates the quality of BEV features across frames. The RCA module integrates reliable feature extraction with a Reliable Memory Bank using a First-In-Last-Out (FILO) buffering strategy and adaptive quality gating. This mechanism selectively preserves trustworthy contextual information while suppressing or reconstructing degraded observations, improving robustness under occlusion, motion blur, and sensor noise.
2. **Temporal Trajectory Planner:** We introduce a Temporal Trajectory Planner based on an LSTM recurrent decoder. This module models long-term temporal relationships and multi-agent interactions within the driving environment. By incorporating historical context into trajectory prediction, the planner can generate smoother, physically consistent, and safety-aware trajectories for both the ego vehicle and surrounding agents.
3. **Semantic and Motion-Guided BEV Refinement:** We further enhance the BEV representation through a Detection and Segmentation Head that jointly integrates motion cues and semantic supervision. This

dual-branch refinement module enriches the BEV features with structural and contextual information, such as drivable areas, obstacles, and scene layout. By embedding both semantic and motion understanding into the BEV space, the framework achieves more accurate perception and provides semantically meaningful representations that support reliable downstream planning.

II. RELATED WORK

A. Semantic-Guided Learning and Scene Understanding

Semantic-guided learning [4], [10] plays a crucial role in enabling autonomous vehicles to understand the driving environment beyond raw geometric cues. By incorporating semantic information such as drivable areas, lane structures and obstacle categories, models can achieve a richer understanding of the scene and make more interpretable planning decisions. Early approaches [31] focused mainly on cross view semantic segmentation or BEV semantic mapping [11], [12] to enhance perception accuracy. However, these methods often treated semantics as an auxiliary output rather than an integral part of the decision-making process. Recent research [7], [8] has begun to integrate semantic cues directly into the feature representation or planning modules, improving contextual reasoning and driving safety. Such semantic-aware scene understanding enables the model to link visual perception with high-level planning intent, ensuring consistency between what the vehicle perceives and how it acts within complex traffic environments.

B. Temporal-Aware and Memory-Gated Learning in Autonomous Driving

Modeling temporal dynamics and long-term memory [11], [13] is vital for autonomous systems to interpret how scenes

evolve, anticipate motion and maintain awareness in continuously changing environments. Unlike single-frame perception [14], [32] which captures only isolated moments, temporal reasoning enables models to follow object motion, anticipate future states and maintain stable awareness in changing environments. Earlier approaches [11], [12] combined features from nearby frames or used temporal attention to improve continuity but often struggled with long-term consistency and noisy information. Later methods [13] introduced recurrent memory modules building on long short-term memory, yet many still rely on fixed time ranges. Building adaptive memory systems that can selectively preserve valuable information remains essential for achieving consistent perception and reliable motion planning in complex driving conditions.

C. Unified BEV Representation for Perception and Planning

A unified bird’s-eye view (BEV) representation [4], [12]

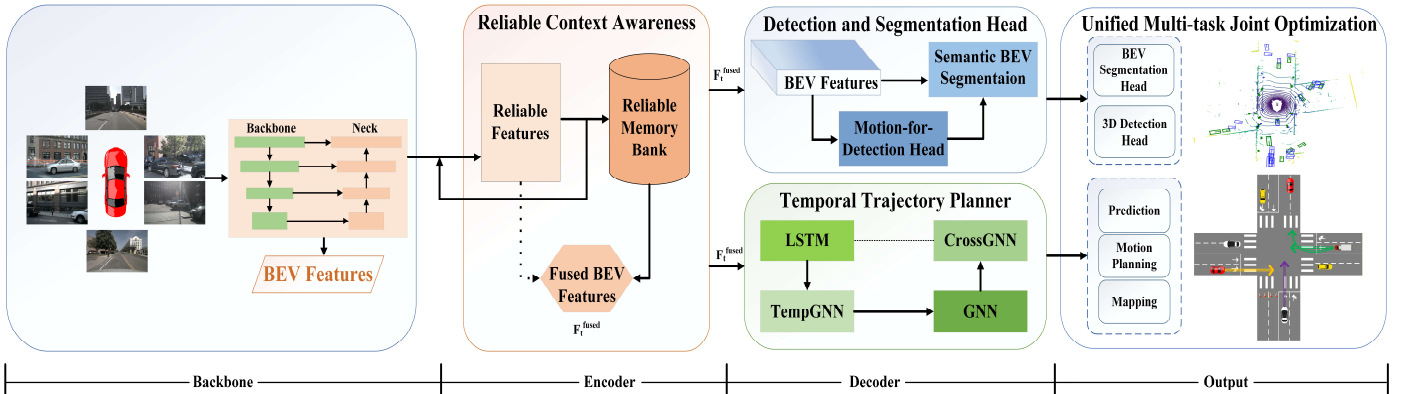


Fig. 2. Overview of the proposed RCT-AD framework. Multi-view camera images are encoded into a unified Bird’s-Eye-View (BEV) representation by the perception backbone. The BEV features are then processed by the Reliable Context Awareness (RCA) module, which evaluates frame reliability and selectively stores reliable features in a FILO-based Reliable Memory Bank, while unreliable observations are reconstructed using historical reliable features. The refined BEV representation is subsequently fed into the Detection and Segmentation Head for semantic segmentation and 3D object detection, and into the Temporal Trajectory Planner, which uses an LSTM-based decoder to model temporal dynamics and generate future trajectories (denotes yellow line in the output), motion states for planning (denotes green line in the output) and mapping (denotes purple line in the output).

III. METHODOLOGY

RCT-AD is a semantically guided and memory-gated end-to-end autonomous driving framework designed to unify perception, temporal reasoning and planning within a single coherent architecture. Unlike existing end-to-end systems such as BridgeAD [7], UniAD [4], GenAD [8] which rely on multi-step query alignment or SparseDrive [6], which emphasizes sparse perception efficiency, RCT-AD explicitly integrates adaptive temporal memory, semantic-level supervision and continuous spatiotemporal reasoning to achieve both robustness and interpretability in dynamic driving environments.

A. Multi-view Adaptive Backbone

The perception backbone of RCT-AD extends the SparseDrive [6] paradigm by constructing a multi-view adaptive encoder that simultaneously handles segmentation, detection, prediction, planning and mapping. Camera images

provides a structured spatial foundation that enables seamless interaction between perception [13] and planning [10] in modern autonomous driving frameworks. By transforming features from multiple cameras [11], [14] into a common spatial space, BEV enables consistent understanding of the environment for detection, mapping, and trajectory prediction. Early BEV methods [11], [12], [15] focused mainly on perception, while later works extended it to motion forecasting and planning. However, many frameworks [6], [10] still treat perception and planning as separate stages, sharing BEV features but without joint optimization. This weak connection limits ability of the model to learn consistent spatial and dynamic relationships between the environment and driving actions. Developing a unified BEV representation that supports multi-task learning, semantic reasoning and temporal stability is essential for achieving more robust and interpretable autonomous driving.

from multiple views are processed by a shared backbone ResNet-50 [25], followed by a deformable neck [26] that converts per view features into BEV tokens [33]. Unlike BridgeAD [7], which relies on a single detection head, RCT-AD deploys five concurrent heads: segmentation, detection, prediction, planning and mapping on a shared BEV latent representation, facilitating coordinated gradient alignment and holistic task optimization.

The multi-view encoder can be formulated as:

$$F_{BEV} = Proj_{BEV} \left(Neck \left(Backbone \left(\{I_i\}_{i=1}^N \right) \right) \right) \quad (1)$$

Where I_i are multi-view images and F_{BEV} is the unified BEV representation that serves all downstream tasks. This shared BEV ensures spatial consistency and semantic grounding across detection and planning tasks.

B. Reliable Context Awareness

RCT-AD incorporates a Reliable Context Awareness (RCA)

mechanism to improve the temporal stability of BEV representations. In real-world driving environments, camera observations are often affected by occlusions, motion blur, illumination changes, and sensor noise. When these unreliable observations are directly aggregated across frames, they can introduce corrupted features that negatively impact perception and planning performance. To mitigate this problem, the RCA module evaluates the reliability of BEV features at each frame and selectively retains trustworthy contextual information through a reliability-guided memory update strategy. By filtering out noisy inputs while preserving reliable features, the framework maintains more stable and consistent scene representations over time.

RCA includes two coordinated modules: (1) a short-term Reliable Features block, which scores incoming frames and, when necessary, repairs them through a bounded meta-update with a FILO buffering and (2) a long-term Reliable Memory Bank, which preserves stable object representations using reliability-based decay. A shared reliability signal controls how information moves and interacts between these two modules.

1. Reliable Features (Short-Term): For each incoming frame t , the perception backbone generates a BEV feature map f_t . RCA computes a reliability score R_t for each incoming frame by combining multiple quality indicators that reflect the consistency and reliability of the BEV features:

$$R_t = \alpha_1 IoU_t + \alpha_2 Conf_t + \alpha_3 (1 - H_t) + \alpha_4 S_t + \alpha_5 P_t \quad (2)$$

Where IoU_t measures spatial alignment with the previous BEV map, $Conf_t$ is the mean detection confidence, H_t denotes segmentation entropy, S_t reflects instance-level temporal stability and P_t captures image clarity from exposure and blur statistics. Each indicator is normalized to $[0, 1]$, and the weights satisfy $\sum_i \alpha_i = 1$, so that $R_t \in [0, 1]$. The weights $\{\alpha_i\}$ are calibrated on the nuScenes validation set (Section IV-D analyzes their sensitivity).

A reliability threshold τ determines how the current frame is processed:

1. $R_t \geq \tau$: the frame is considered reliable and its features are transferred to the long-term Reliable Memory Bank for future fusion.
2. $R_t < \tau$: the frame is unreliable and is passed to a bounded repair loop before it is allowed to enter memory.

Bounded meta-update: Let $f_t^{(0)} = f_t$ denote the degraded feature and $R_t^{(0)} = R_t$ its score. At iteration k , RCA retrieves the most reliable historical feature from the Reliable Memory Bank,

$$m^{*(k)} = \arg \max_{m \in B} R_m \quad (3)$$

warps it to the current ego-pose, and blends it with the current estimate:

$$f_t^{(k)} = \lambda^{(k)} f_t^{(k-1)} + (1 - \lambda^{(k)}) \text{Warp}(f_{m^{*(k)}}, \Delta \text{pose}),$$

$$\lambda^{(k)} = \frac{R_t^{(k-1)}}{R_t^{(k-1)} + R_{m^{*(k)}}} \quad (4)$$

The repaired feature is then re-scored by Eq. (2), yielding $R_t^{(k)}$. The Meta-Update terminates when the repaired frame

becomes reliable, $R_t^{(k)} \geq \tau$, in which case the frame is treated as reliable and fused as above. If reliability is not restored within K_r Meta-Update iterations, RCA falls back to the warped most-reliable historical feature, trusting consistent history over the corrupted current observation. Because each iteration re-retrieves the current best historical feature and blends in higher-reliability context, the score tends to increase across iterations; capping at K_r guarantees termination and preserves the real-time budget. The short-term buffer is updated only along the Meta-Update path:

$$M_t = \begin{cases} \text{Push}(M_{t-1}, \tilde{f}_t), & R_t < \tau \\ M_{t-1}, & R_t \geq \tau \end{cases} \quad (5)$$

Where $\tilde{f}_t = f_t^{(k^*)}$ is the accepted feature at the terminating iteration (or the historical fallback). Each buffer entry is stored as a tuple (f_i, R_i, a_i) of feature, reliability, and age. The importance of an entry decays exponentially with its age, $w_i = \exp(-\beta a_i)$. When the buffer is full, the oldest or least-reliable entry is evicted, while highly reliable entries are refreshed and promoted. This aging-refresh policy keeps strong, consistent frames active while automatically discarding weaker ones.

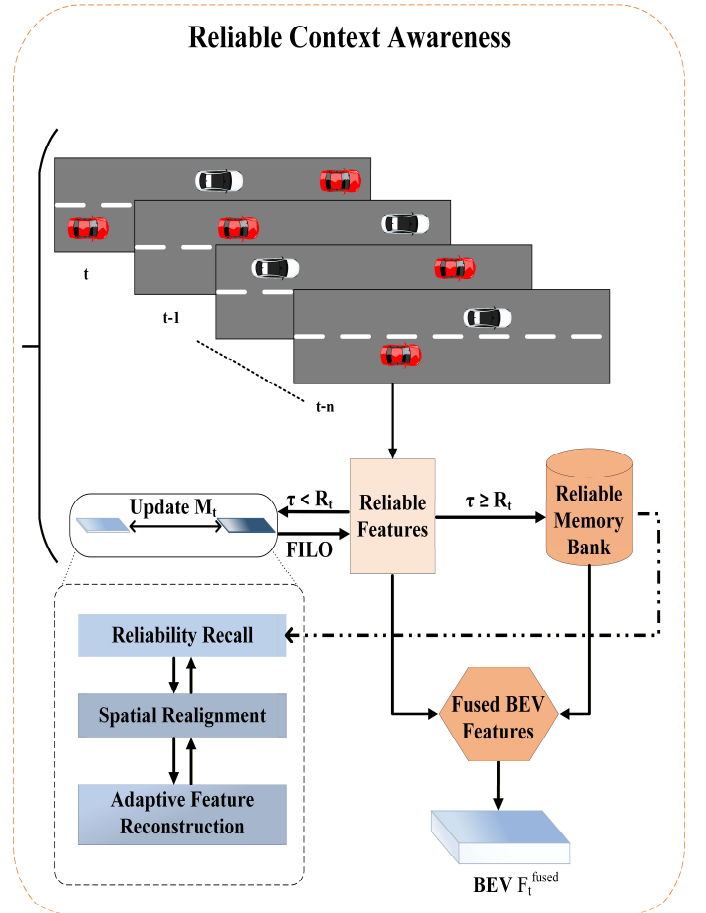


Fig. 3. Reliable Context Awareness mechanism, the BEV features across frames initially enter in the proposed RCA block. Reliable Features block checks the reliability. Reliable frames store in the Reliable memory bank for further process and unreliable frames reconstruct the BEV features by integrating the most trustworthy frame from Reliable memory bank.

2. Reliability Fusion (Long-term): The Reliable Memory Bank maintains long-term consistency for moving objects and scene elements. Each tracked instance i has an embedding h_t^i that updates over time using an exponential decay weighted by its reliability:

$$h_{t+1}^i = \gamma_t^i h_t^i + (1 - \gamma_t^i) f_t^i, \quad \gamma_t^i = g(R_t^i) \quad (6)$$

Here $g(\cdot)$ is a learned reliability-gating function implemented as a sigmoid-activated single-layer MLP trained jointly with the detection and planning objectives, that maps per-instance reliability to a blending factor in $[0, 1]$. Reliable observations therefore dominate updates, while uncertain ones contribute softly without destabilizing trajectories.

At decoding time, all stored instance embeddings are aggregated through reliability-weighted fusion and refined by channel attention:

$$F_t^{fused} = \sum_{i=1}^N \omega_i f_t^i, \quad \omega_i = \frac{R_t^i}{\sum_j R_t^j} \quad (7)$$

$$F_t^{final} = CA(F_t^{fused}, f_t) \quad (8)$$

A Channel-attention module [28] highlights feature that stay consistent over time and reduces the impact of unstable ones, generating the final refined representation F_t^{final} used for detection, mapping and planning.

Algorithm 1 Reliable Context Awareness mechanism

Inputs:

- i. BEV feature of current frame f_t .
- ii. Reliability components $\{IoU_t, Conf_p, H_t, S_t, P_t\}$.
- iii. Previous short-term memory M_{t-1} .
- iv. Reliable Memory Bank \mathcal{B}_{t-1} .
- v. Reliability threshold $\tau = 0.85$.
- vi. Max Meta-update iterations K_r .

Outputs:

- i. Updated Reliable Features M_t .
- ii. Updated Reliable Memory Bank \mathcal{B}_t .
- iii. Fused BEV representation F_t^{final} .

Steps:

1. Reliability Computation: compute R_t via Eq. (2)
2. Routing: if $R_t \geq \tau$ then store f_t in Reliable Memory Bank \mathcal{B}_t ; set $M_t \leftarrow M_{t-1}$; go to Step 5.
3. Bounded Meta-Update: set $f_t^{(0)} \leftarrow f_t, R_t^{(0)} \leftarrow R_t$
for $k = 1$ to K_r do

retrieve $m^{*(k)} = \operatorname{argmax}_{m \in \mathcal{B}} R_m$; warp to current pose;

compute $f_t^{(k)}$ and $\lambda^{(k)}$ via Eq. (4)

re-score $R_t^{(k)}$ via Eq. (2);

if $R_t^{(k)} \geq \tau$ then $\tilde{f}_t \leftarrow f_t^{(k)}$; break.

end for

if Meta-Update did not coverage, then $\tilde{f}_t \leftarrow$

$Warp(f_{m^{*(k)}}, \Delta pose)$ (historical fallback)

Push \tilde{f}_t into buffer: $M_t \leftarrow Push(M_{t-1}, \tilde{f}_t)$; store \tilde{f}_t in

\mathcal{B}_t .

4. Memory Maintenance: if $|M_t| > \text{capacity}$, then evict

oldest or least-reliable entry;

for each $(f_i, R_i, a_i) \in M_t$: if $R_i > \text{mean}(R)$

then promote entry; else apply decay weight

$w_i = \exp(-\beta a_i)$.

5. Aggregate and refine: compute F_t^{fused} via Eq. (7);

$F_t^{final} = CA(F_t^{fused}, f_t)$ via Eq. (8).

C. Temporal Trajectory Planner

Temporal Trajectory Planner is a core contribution of RCT-AD, acting as the central reasoning module for predicting smooth and temporal-aware driving trajectories. Temporal trajectory planner combines temporal sequence encoding, spatial interaction reasoning and multi-modal trajectory decoding in a unified recurrent-attention design. Unlike static planners such as SparseDrive [6], BridgeAD [7], GenAD [8] temporal trajectory planner preserves a temporal memory across frames and adaptively models cooperative or competitive interactions among agents, ensuring consistent and context-aware planning in dynamic traffic scenarios.

Temporal Sequence Encoding: Given a sequence of BEV embeddings $Q_{1:t}^m \in \mathbb{R}^{T \times C}$ for motion mode m , Temporal trajectory planner employs a single layer LSTM to capture temporal dependencies and preserve motion continuity:

$$(H_t^m, (h_t, c_t)) = LSTM(Q_t^m, (h_{t-1}, c_{t-1})) \quad (9)$$

Where H_t^m denotes the aggregated spatiotemporal feature and (h_t, c_t) represent hidden and cell states. In our implementation, the LSTM hidden dimension is set to $C=256$, equal to the BEV embedding dimension. This mechanism allows temporal propagation of motion semantics such as acceleration, turning, and lane merging.

Spatial Interaction Reasoning: The temporal embeddings are refined through graph-attention modules that encode spatial dependencies between the ego-agent, surrounding vehicles and the map. The overall operation can be formulated as:

$$Z_t^m = CrossGNN(TempGNN(H_t^m, A), M_{map}) \quad (10)$$

Where A and M_{map} denotes agent and map features respectively. *TempGNN* model refers to inter-agent temporal dynamics such as yielding, overtaking etc. while *CrossGNN*

integrates topological priors such as lane geometry and drivable area constraints. This dual-attention structure enables Temporal trajectory planner to reason jointly over when (temporal) and where (spatial) motion decisions occur.

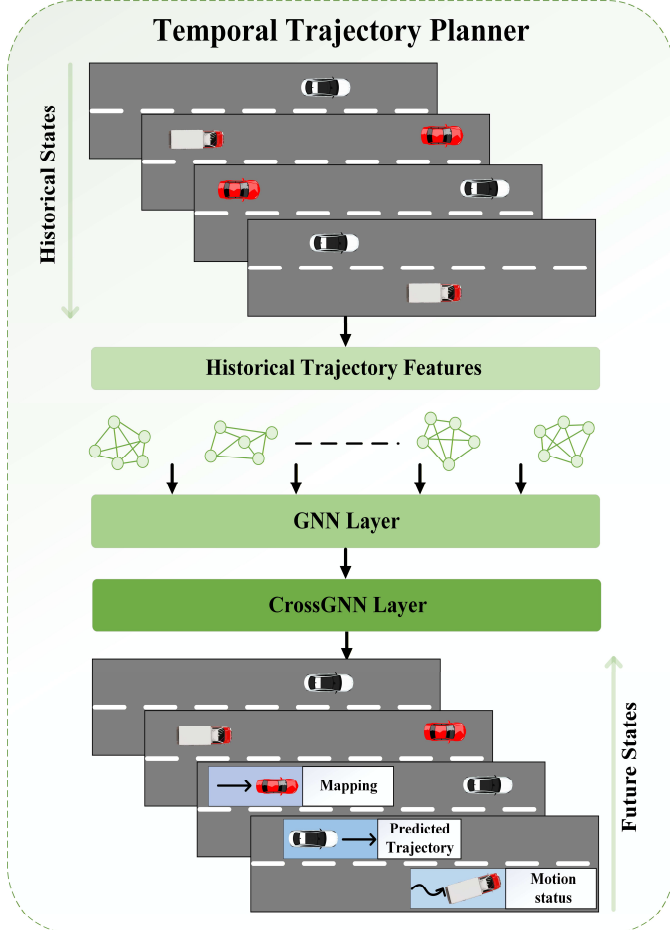


Fig. 4. Temporal trajectory planner encodes historical BEV-based agent states and models using GNN and Cross-GNN layers to capture temporal features. The temporal features are subsequently utilized to predict future trajectories and motion status, enabling robust planning and mapping in dynamic driving environments.

Multi-modal Trajectory Decoding: The interaction-enriched representation Z_t^m is decoded through three lightweight MLP heads to generate multi-modal trajectory hypotheses:

$$\hat{p}^m = \text{softmax}(\Psi_{cls}(Z_t^m)), \hat{y}^m = (\Psi_{reg}(Z_t^m)), \hat{s}^m = (\Psi_{stat}(Z_t^m)) \quad (11)$$

Where Ψ_{cls} , Ψ_{reg} , Ψ_{stat} represent the maneuver classification, waypoint regression and motion-state estimation heads, respectively. These branches deliver complementary supervisory cues, improving both the accuracy of trajectory geometry and the diversity of driving behaviors.

Planning Objective: Temporal trajectory planner is trained with a multi-task objective that jointly optimizes maneuver recognition, trajectory regression and motion status prediction:

$$\mathcal{L}_{plan} = \lambda_{cls} \mathcal{L}_{CE}(\hat{p}^m, p^m) + \lambda_{reg} \|\hat{y}^m - y^m\|_1 + \lambda_{stat} \mathcal{L}_{CE}(\hat{s}^m, s^m) \quad (12)$$

Where p^m , y^m and s^m denote the ground-truth maneuver label, future waypoints and motion state, respectively.

D. Detection and Segmentation Head

Detection and Segmentation Head serves as the perception refinement stage of RCT-AD, designed to jointly leverage motion and semantic cues for better BEV understanding. Instead of handling detection and segmentation separately [13], [16], [20], [31], [34], Detection and Segmentation Head merges them within a unified refinement layer that enriches BEV features with temporal motion and scene semantics. This integration enhances object boundaries, stabilizes localization under motion blur or occlusion, and maintains scene-level consistency between perception and planning.

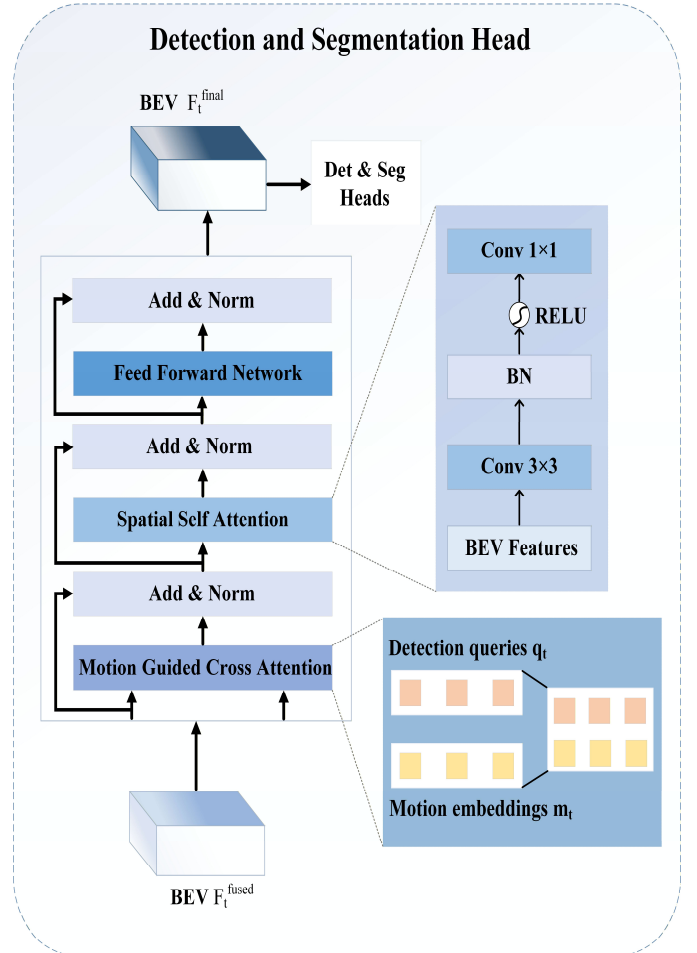


Fig. 5. Detection and Segmentation Head refines fused BEV features by jointly incorporating semantic and motion information. The refined features are shared by the detection and segmentation heads, providing consistent perceptual cues to support reliable downstream planning.

Detection and Segmentation Head consists of two complementary parts: Motion-for-Detection Adaptive Fusion, which integrates motion cues into detection queries using motion-based cross-attention to ensure smoother and more consistent object tracking over time. Semantic BEV Segmentation for guided supervision, which introduces

semantic information like drivable areas, lanes, obstacles, cars, trucks etc. into the shared BEV space to guide and stabilize both detection and segmentation.

Motion-for-Detection Adaptive Fusion: RCT-AD integrates a Motion-for-Detection Head block, a compact transformer module that embeds temporal motion information into the detection decoder. This enables the model to enhance object localization by leveraging motion context, improving performance in dense or occluded environments. The Motion-for-Detection head performs motion-guided cross attention, where motion embeddings m_t are concatenated with detection queries q'_t :

$$q'_t = \text{Attn}(q_t + \varphi(m_t)) \quad (13)$$

Here, φ is a learned projection aligning temporal motion with spatial features and q'_t is the motion enhanced detection query.

Semantic BEV Segmentation for Guided Supervision: RCT-AD integrates a BEV Semantic Segmentation Head directly into the multi-task pipeline. This head reshapes BEV tokens [33] into a spatial grid and predicts per-cell classes such as roads, lanes, drivable areas, pedestrians, etc. enforcing semantic alignment between perception and planning.

$$\hat{Y}_{seg} = \text{Conv}_{1 \times 1} \left(\text{ReLU} \left(\text{BN} \left(\text{Conv}_{3 \times 3} (F_{BEV}) \right) \right) \right) \quad (14)$$

This semantic head provides rich topological priors that guide both detection and planning heads, ensuring that predicted trajectories respect physical and drivable constraints.

E. Unified Multi-Task Joint Optimization

RCT-AD employs a Unified Multi-Task Joint Optimization paradigm that combines segmentation, detection, prediction, planning and mapping within a single end-to-end training objective. This strategy allows shared BEV representations to be refined through gradients from every subtask, thereby ensuring consistent semantics, spatial alignment and temporal coherence across the entire driving pipeline. The overall objective is formulated as:

$$\begin{aligned} \mathcal{L}_{total} = & \lambda_{det} \mathcal{L}_{det} + \lambda_{seg} \mathcal{L}_{seg} + \lambda_{plan} \mathcal{L}_{plan} + \\ & \lambda_{map} \mathcal{L}_{map} + \lambda_{mem} \mathcal{L}_{mem} \end{aligned} \quad (15)$$

Where \mathcal{L}_{det} , \mathcal{L}_{seg} , \mathcal{L}_{plan} , \mathcal{L}_{map} , \mathcal{L}_{mem} denote respectively detection loss, semantic segmentation loss, trajectory supervision loss, vectorized-mapping loss, and temporal-consistency loss across frames.

IV. EXPERIMENTS

A. Experimental Settings

We evaluate the proposed RCT-AD framework on the nuScenes dataset. The nuScenes [1] benchmark provides 1,000 driving sequences with comprehensive 2 Hz annotations, six camera feeds, and detailed 3D and semantic labels, offering a robust testbed for assessing perception, prediction and planning capabilities. RCT-AD processes multi-view camera images through a unified Bird’s-Eye-View (BEV) backbone [25]. Within this framework, the RCA module enhances perceptual stability against occlusions and motion blur, while the

Detection and Segmentation Head further refines the features by incorporating semantic and motion information.

For open-loop assessment, we adopt established protocols from VAD [5] and BridgeAD [7], reporting L2 displacement error, collision rate, and standard nuScenes scores including mean Average Precision (mAP), nuScenes Detection Score (NDS), and BEV segmentation Intersection-over-Union (IoU). All evaluations are conducted on the nuScenes validation set.

B. Implementation Details

RCT-AD forecasts a 3-second future trajectory for the ego vehicle and a 6-second prediction for the surrounding agents, which is equal to $T_{plan} = 6$ and $T_{mot} = 12$ future steps in total. For temporal modeling, we use a motion-history length of $T_{m2m} = 6$ previous frames for motion prediction and a planning-history length of $T_{p2p} = 3$ frames for planning, while RCA maintains a memory queue of the past $K = 6$ fused BEV representations. The perception backbone is based on a multi-view BEV encoder with ResNet-50 [25] and an input size of 256×704 as the tiny variant of RCT-AD-T, while a larger variant RCT-AD-L uses ResNet-101 with 512×1408 resolution. Detection and Segmentation Head and Temporal Trajectory Planner work in the same BEV latent space and they provide the functions of semantic refinement and interactive temporal planning, respectively. RCT-AD employs AdamW [27] with a cosine schedule, starting from a learning rate of 1×10^{-4} , a weight decay of 1×10^{-3} and is trained with a batch size of 8 for 50 epochs. The training is done in two parts; the first one is the perception-only pre-training and the second is the unified end-to-end optimization.

C. Performance Comparison

Motion planning comparison on nuScenes dataset: Table I summarizes the motion-planning performance of several representative end-to-end autonomous driving frameworks. The comparison includes L2 displacement error and collision rate evaluated at 1 s, 2 s, and 3 s prediction horizons. Recent works including VAD [5], SparseDrive [6] and GenAD [8] use a lighter R50 backbone [25] and show higher prediction error and more collisions. Comparing with the baseline, our RCT-AD-T (Tiny) performs slightly better. Prior works including UniAD [4] and BridgeAD [7] use an R101 backbone and provide more stable trajectories. Both variants of our model are competitive with or better than the baselines; RCT-AD-L (large) achieves the lowest average L2 displacement error and collision rate, indicating strong long-horizon accuracy and safety.

Motion prediction comparison on nuScenes dataset: Table II presents motion-prediction results for cars and pedestrians using average displacement error (ADE), final displacement error (FDE), end-point accuracy (EPA), and miss rate (MR), where lower ADE, FDE, and MR and higher EPA indicate better performance. Compared with other baselines models, RCT-AD-T demonstrates superior performance with the R50 backbone [25], achieving reduced prediction errors and improved endpoint accuracy. When equipped with the R101 backbone, RCT-AD-L achieves the highest overall accuracy, exceeding the performance of UniAD [4] and BridgeAD-B [7] across all metrics.

3D detection comparison on nuScenes dataset: Table III presents a comparison of various 3D detection approaches applied to the nuScenes using mAP and NDS metrics. The best

performing model with ResNet-50 backbone [25] is RCT-AD-T with mAP of 44.2 and NDS of 55.6, which exceeding the results of VAD [5], SparseDrive [6] and BridgeAD-S [7]. When using

ResNet-101 backbone, RCT-AD-L presents the most significant overall performance, achieving 52.9 mAP and 61.5 NDS, which is better than UniAD [4], BridgeAD-B [7] and BEVFormer [11].

TABLE I

MOTION PLANNING COMPARISON ON NUSCENES [1] DATASET. + INDICATES EVALUATION WITH THE OFFICIAL CHECKPOINT. UNIAD [4] IS MEASURED ON NVIDIA TESLA A100. FOR OTHER METHODS WE USE NVIDIA RTX A6000 GPU WITH A BATCH SIZE OF 1.

Method	Backbone	L2 (m) ↓				Collision Rate (%) ↓			
		1s	2s	3s	Avg	1s	2s	3s	Avg
GenAD [8]	R50	0.36	0.83	1.55	0.91	0.06	0.23	1.00	0.43
VAD+ [5]	R50	0.41	0.70	1.05	0.72	0.03	0.19	0.43	0.21
SparseDrive+ [6]	R50	0.30	0.58	0.95	0.61	0.01	0.05	0.23	0.10
RCT-AD-T (Ours)	R50	0.29	0.57	0.93	0.59	0.01	0.04	0.18	0.07
UniAD+ [4]	R101	0.45	0.70	1.04	0.73	0.05	0.17	0.71	0.31
BridgeAD [7]	R101	0.28	0.55	0.92	0.58	0.00	0.04	0.20	0.08
RCT-AD-L (Ours)	R101	0.23	0.52	0.89	0.54	0.01	0.03	0.15	0.06

TABLE II

MOTION PREDICTION COMPARISON ON NUSCENES [1] DATASET. + INDICATES EVALUATION WITH THE OFFICIAL CHECKPOINT. WE EVALUATE TWO MAIN CATEGORIES, CARS AND PEDESTRIAN RESPECTIVELY.

Method	Backbone	ADE (m) ↓		FDE (m) ↓		EPA ↑		MR (%) ↓	
		Car	Ped	Car	Ped	Car	Ped	Car	Ped
SparseDrive+ [6]	R50	0.62	0.72	0.99	1.07	0.48	0.41	0.14	0.14
BridgeAD-S [7]	R50	0.62	0.70	0.98	0.99	0.50	0.44	0.13	0.13
RCT-AD-T (Ours)	R50	0.61	0.67	0.95	0.98	0.51	0.46	0.12	0.11
ViP3D [29]	R101	2.05	-	2.84	-	0.23	-	0.25	-
UniAD+ [4]	R101	0.71	0.78	1.02	1.05	0.46	0.35	0.15	0.12
BridgeAD-B [7]	R101	0.60	0.70	0.96	0.98	0.52	0.45	0.13	0.12
RCT-AD-L (Ours)	R101	0.58	0.66	0.94	0.98	0.56	0.47	0.12	0.12

TABLE III

3D DETECTION COMPARISON ON NUSCENES [1] DATASET. + INDICATES EVALUATION WITH OFFICIAL CHECKPOINT.

Method	Backbone	mAP	NDS	Car	Truck	Bus	Trailer	C. vehicle	Ped	Motor cycle	Bi-cycle	Barrier	T. Cone
VAD+ [5]	R50	27.3	39.7	44.5	18.6	32.1	-	-	38.7	23.1	41.4	27.4	47.2
SparseDrive+ [6]	R50	41.8	52.5	59.8	44.2	49.1	-	-	52.7	51.4	52.3	47.4	61.1
BridgeAD-S [7]	R50	42.3	53.4	64.3	44.8	49.2	-	-	53.3	51.7	50.6	46.7	62.4
RCT-AD-T (Ours)	R50	44.2	55.6	65.7	49.1	49.7	-	-	58.1	52.6	53.2	47.1	66.9
BEVFormer [11]	R101	41.6	51.7	59.6	44.4	48.8	-	-	51.9	50.8	51.2	47.5	61.8
UniAD [4]	R101	38.0	49.8	53.4	39.5	42.9	-	-	47.2	45.3	50.1	46.3	55.3
BridgeAD-B [7]	R101	50.7	59.4	76.2	47.2	49.8	-	-	67.4	59.1	61.9	68.3	77.1
RCT-AD-L(Ours)	R101	52.9	61.5	79.1	47.9	52.2	-	-	72.5	63.6	62.2	69.7	81.8

Segmentation comparison on nuScenes dataset: Table IV demonstrates that RCT-AD model achieves the highest in mIoU metrics over both backbones. By using the R50 backbone [25], RCT-AD-T reaches 49.8 mIoU, which is a big difference compared to VPN [31] and LSS [12] which are still lower than

RCT-AD-T. When the R101 backbone is used, RCT-AD-L achieves the best result of 52.3 mIoU, surpassing BEVFormer [11] and Simple-BEV [32]. Overall, RCT-AD consistently delivers superior BEV segmentation performance on the nuScenes dataset [1].

TABLE IV
SEGMENTATION COMPARISON ON NUSCENES [1] DATASET.

Method	Backbone	Input Size	mIoU
VPN [31]	R50	256 × 704	43.8
LSS [12]	R50	256 × 704	45.0
RCT-AD-T (Ours)	R50	256 × 704	49.8
BEVFormer [11]	R101	900 × 1600	47.3
Simple-BEV [32]	R101	448 × 800	47.4
RCT-AD-L (Ours)	R101	512 × 1408	52.3

D. Ablation Study

Multi object tracking performance: Table V presents multi-object-tracking performance using average multi-object tracking accuracy (AMOTA), average multi-object tracking precision (AMOTP), recall, and identity switches (IDS), where

higher AMOTA and recall and lower AMOTP and IDS indicate better tracking. RCT-AD-T outperforms all R50 baselines, showing more stable tracking in dynamic scenes. With the R101 backbone, RCT-AD-L achieves even stronger results, obtaining the highest AMOTA, lowest AMOTP and fewer IDS.

Component-wise performance analysis: Table VI visualizes ablation studies that RCA improves overall perception and prediction, while the Temporal Trajectory Planner significantly enhances planning accuracy and NDS. The Detection and Segmentation Head improves perception but does not impact trajectory prediction. The complete model achieves the highest mAP, NDS, IoU, ADE, FDE and EPA, indicating that both modules are critical and work aggregately within the RCT-AD framework.

Performance comparison with reliable context awareness: Table VII evaluates the contributions of the Reliable Features and the FILO strategy within RCA. Incorporating FILO-based short-term memory leads to clear improvements in NDS, indicating that prioritizing high-reliability frames strengthens temporal consistency.

TABLE V
PERFORMANCE COMPARISON WITH MULTI OBJECT TRACKING.

Method	Backbone	AMOTA ↑	AMOTP ↓	Recall ↑	IDS ↓
ViP3D [29]	R50	0.217	1.625	0.363	-
SparseDrive [6]	R50	0.386	1.254	0.499	886
BridgeAD-S [7]	R50	0.398	1.232	-	639
RCT-AD-T (Ours)	R50	0.415	1.188	0.530	578
UniAD [4]	R101	0.359	1.320	0.467	906
BridgeAD-B [7]	R101	0.512	1.080	-	544
RCT-AD-L (Ours)	R101	0.527	1.004	0.519	503

TABLE VI
COMPONENT-WISE ABLATION OF RCT-AD ON THE NUSCENES VALIDATION SET (RCT-AD-L BACKBONE). ✓ and ✗ indicate whether a component is enabled or disabled; - indicates the metric is not applicable to that configuration.

ID	RCA	Temporal Trajectory Planner	Detection and Segmentation Head	Detection		Segmentation	Motion Prediction		
				mAP	NDS	IoU	ADE ↓	FDE ↓	EPA ↑
1	✓	✗	✗	-	-	-	0.71	1.53	0.38
2	✓	✗	✓	48.4	53.0	49.7	0.71	1.53	0.38
3	✓	✓	✗	49.6	59.7	51.1	0.67	1.04	0.46
4	✓	✓	✓	52.9	61.5	52.3	0.62	0.96	0.51

TABLE VII
PERFORMANCE COMPARISON WITH RELIABLE CONTEXT AWARENESS.

ID	RCA	FILO	NDS ↑
1	✓	✗	52.0
2	✗	✓	48.1
3	✓	✓	55.6

Performance comparison with different threshold (τ) score: Table VIII evaluates the impact of different reliability threshold scores in the RCA module. When the threshold is set to 0.65, including those with lower reliability, which introduces noise and results in relatively lower performance. Increasing the threshold to 0.75 filters out some of these unreliable frames, leading to improved stability and better performance. The best results are achieved when the threshold is 0.85, where only

highly reliable frames are retained, producing robust performance.

TABLE VIII

PERFORMANCE COMPARISON WITH DIFFERENT THRESHOLD SCORE.

ID	Threshold Score (τ)	mAP \uparrow	NDS \uparrow
1	0.65	39.2	48.6
2	0.75	42.9	51.1
3	0.85	44.2	55.6

Reliability Coefficient Sensitivity Analysis: To examine whether the selected coefficient setting $(\alpha_1, \alpha_2, \alpha_3, \alpha_4, \alpha_5) = (0.25, 0.30, 0.15, 0.20, 0.10)$ is robust rather than overly

sensitive to a specific configuration, we conduct a sensitivity analysis on the two most influential terms, namely geometric IoU (α_1) and detection confidence (α_2). Specifically, each of these two coefficients is perturbed by ± 0.10 around its selected value, while the remaining coefficients are proportionally adjusted to maintain the simplex constraint $\sum_i \alpha_i = 1$. This analysis allows us to evaluate whether moderate changes in the reliability-score composition lead to significant performance fluctuations. As shown in [Table IX](#), validation NDS changes by less than 0.7 across all tested perturbations, with the selected setting achieving the best score of 55.6. Reducing α_2 causes the largest drop, confirming detection confidence as the most influential reliability cue. Perturbations of α_1 lead to only minor changes, indicating that geometric IoU is useful but not dominant.

TABLE IX

SENSITIVITY ANALYSIS OF α_1 AND α_2 ON THE NUSCENES VALIDATION SET. BEST RESULT IS MARKED IN BOLD.

Variant	α_1 (IoU)	α_2 (Conf)	α_3 (1-H)	α_4 (S)	α_5 (P)	NDS \uparrow
$-\alpha_1$	0.15	0.30	0.15	0.20	0.10	55.1
$+\alpha_1$	0.35	0.30	0.15	0.20	0.10	55.0
$-\alpha_2$	0.25	0.20	0.15	0.20	0.10	54.9
$+\alpha_2$	0.25	0.40	0.15	0.20	0.10	55.3
Selected (Default)	0.25	0.30	0.15	0.20	0.10	55.6

E. Computational Efficiency Analysis

[Table X](#) compares computational efficiency across representative end-to-end driving frameworks. RCT-AD achieves a strong balance of speed and accuracy, offering faster inference than UniAD [\[4\]](#) while maintaining competitive

memory usage. GFLOPs and parameter of RCT-AD count remain modest relative to performance gains, enabling a higher throughput of 7.2 FPS. These results demonstrate that RCT-AD delivers improved planning and perception performance without incurring excessive computational overhead.

TABLE X

RUNTIME ANALYSIS AND MEMORY REQUIREMENTS.

Method	Memory (GB)	Inference Time (ms)	GFLOPs	Params (M)	FPS
UniAD [4]	50	555.6	1709	125.0	1.8
SparseDrive [6]	15.2	163.9	192	85.9	6.1
BridgeAD [7]	17.6	157.2	485	129.4	6.4
RCT-AD (Ours)	19.5	138.6	379	99.56	7.2

F. Visualization

[Fig. 6](#) provides qualitative results demonstrating how RCT-AD integrates reliable context-aware perception, semantic BEV reasoning and temporal planning within a unified end-to-end framework. The multi-view camera visualizations show stable and consistent object detection across all surround views, even under occlusions and complex urban layouts. This robustness is enabled by RCA, which selectively preserves high-quality BEV features and reconstructs unreliable observations through

reliability-gated short-term reliable features and long-term reliable memory.

The BEV visualizations further highlight the contribution of the Detection and Segmentation Head, which injects semantic supervision into the shared BEV space. Lane topology, drivable regions and dynamic agents are represented with clear structural coherence, providing semantically grounded inputs for planning. This semantic refinement improves spatial

consistency and ensures that downstream decisions respect scene geometry and traffic constraints.

For each scenario, RCT-AD generates multiple maneuver-conditioned trajectories (turn left, go straight, turn right). The trajectories are generated by the Temporal Trajectory Planner, which employs a recurrent decoding mechanism to capture long-horizon temporal dynamics and model interactions among

agents. The resulting trajectories are smooth, collision-aware and adaptive to surrounding traffic dynamics and ego speed. In summary, the visualization qualitatively demonstrates that RCT-AD achieves robust perception, interpretable BEV representations and enables temporally consistent multi-modal planning.

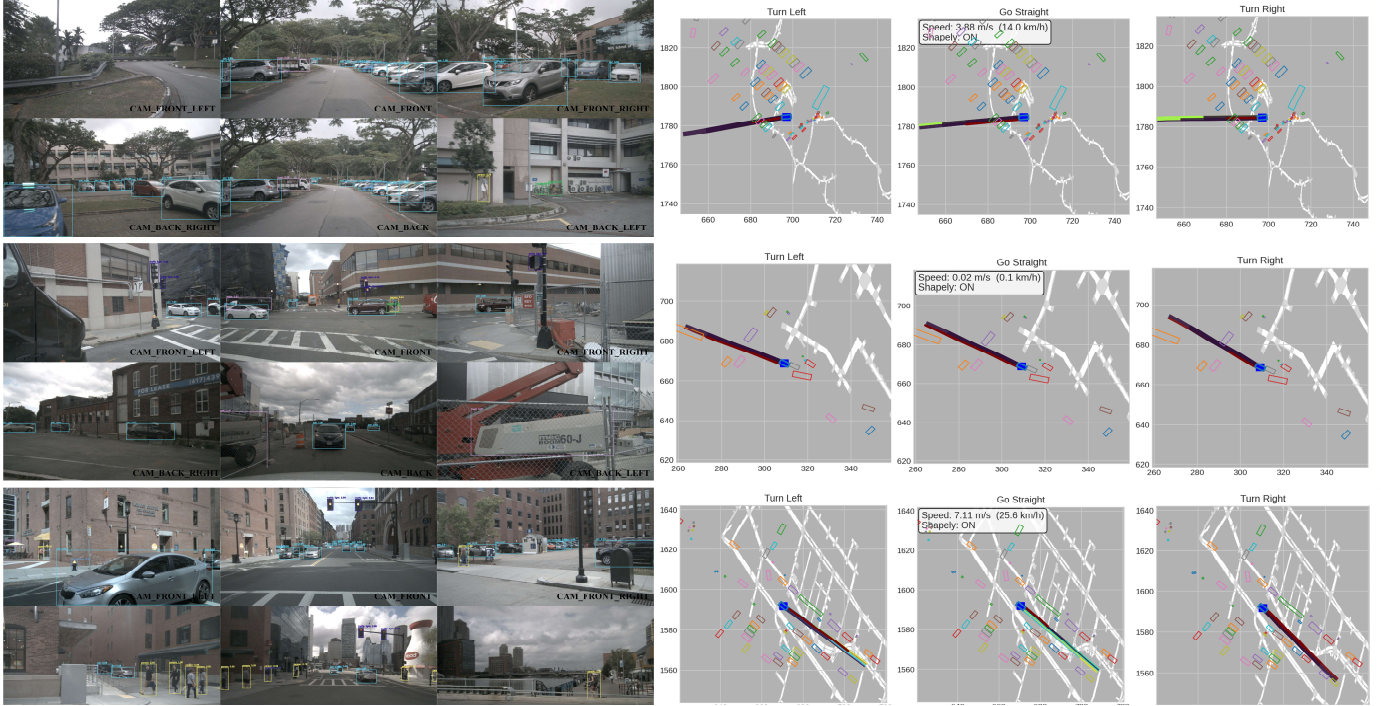


Fig. 6. Qualitative results of the proposed RCT-AD framework demonstrating reliable perception, semantic BEV representation, and temporal trajectory planning under complex urban driving scenarios. The model maintains stable multi-view detection through reliability-aware feature selection (RCA), produces structurally consistent BEV semantic maps with lane and drivable area understanding, and generates collision-aware multi-modal future trajectories using the Temporal Trajectory Planner.

V. CONCLUSION

We present RCT-AD, a reliable, context-aware temporal-planning framework for end-to-end autonomous driving that unifies perception, temporal modeling, and motion planning within a shared BEV representation. Unlike prior end-to-end methods that rely on implicit temporal aggregation, RCT-AD explicitly models feature reliability, semantic structure and agent interactions leading to more robust and consistent decision-making in dynamic environments. RCT-AD integrates three key components: (1) RCA, a reliable context-aware mechanism that selectively preserves high-quality BEV features via quality-aware routing and FILO-based short-term memory; (2) Temporal Trajectory Planner, a recurrent planner that captures long-term temporal dependencies and multi-agent behaviors; and (3) Detection and Segmentation Head, which injects semantic and motion cues into BEV refinement to enforce structural consistency. Experiments on nuScenes demonstrate that RCT-AD consistently outperforms state-of-the-art end-to-end driving frameworks across perception, prediction and planning tasks, while maintaining competitive computational efficiency.

A key direction for future work is closed-loop evaluation. While the present study assesses RCT-AD under the standard open-loop nuScenes protocol, we plan to validate planning safety and reliability in interactive, reactive settings using photorealistic closed-loop simulators such as NeuroNCAP [3], which generate safety-critical scenarios in which the planner must continuously plan and execute trajectories. We will further extend RCT-AD to multi-modal sensor fusion with LiDAR and radar, alongside uncertainty-aware [19] reliability modeling and long-horizon scene reasoning to better anticipate rare, safety-critical events, and pursue efficiency-driven optimization and sim-to-real deployment evaluation.

ACKNOWLEDGMENT

The authors would like to thank the College of Computer Science, Chongqing University, for providing the laboratory facilities and experimental resources that supported this research.

REFERENCES

- [1] H. Caesar *et al.*, “nuScenes: A multimodal dataset for autonomous driving,” in *Proc. IEEE/CVF Conf. Comput. Vis. Pattern Recognit. (CVPR)*, 2020, pp. 11621–11631.

- [2] L. Chen, P. Wu, K. Chitta, B. Jaeger, A. Geiger, and H. Li, “End-to-end autonomous driving: Challenges and frontiers,” *IEEE Trans. Pattern Anal. Mach. Intell.*, vol. 46, no. 12, pp. 10164–10183, 2024.
- [3] W. Ljungbergh *et al.*, “NeuroNCAP: Photorealistic closed-loop safety testing for autonomous driving,” in *Proc. Eur. Conf. Comput. Vis. (ECCV)*, 2024, pp. 161–177.
- [4] Y. Hu *et al.*, “Planning-oriented autonomous driving,” in *Proc. IEEE/CVF Conf. Comput. Vis. Pattern Recognit. (CVPR)*, 2023, pp. 17853–17862.
- [5] B. Jiang *et al.*, “VAD: Vectorized scene representation for efficient autonomous driving,” in *Proc. IEEE/CVF Int. Conf. Comput. Vis. (ICCV)*, 2023, pp. 8340–8350.
- [6] W. Sun, X. Lin, Y. Shi, C. Zhang, H. Wu, and S. Zheng, “SparseDrive: End-to-end autonomous driving via sparse scene representation,” in *Proc. IEEE Int. Conf. Robot. Autom. (ICRA)*, 2025, pp. 8795–8801.
- [7] B. Zhang, N. Song, X. Jin, and L. Zhang, “Bridging past and future: End-to-end autonomous driving with historical prediction and planning,” in *Proc. IEEE/CVF Conf. Comput. Vis. Pattern Recognit. (CVPR)*, 2025, pp. 6854–6863.
- [8] W. Zheng, R. Song, X. Guo, C. Zhang, and L. Chen, “GenAD: Generative end-to-end autonomous driving,” in *Proc. Eur. Conf. Comput. Vis. (ECCV)*, 2024, pp. 87–104.
- [9] B. Liao *et al.*, “DiffusionDrive: Truncated diffusion model for end-to-end autonomous driving,” in *Proc. IEEE/CVF Conf. Comput. Vis. Pattern Recognit. (CVPR)*, 2025, pp. 12037–12047.
- [10] Y. Wang, J. He, L. Fan, H. Li, Y. Chen, and Z. Zhang, “Driving into the future: Multiview visual forecasting and planning with world model for autonomous driving,” in *Proc. IEEE/CVF Conf. Comput. Vis. Pattern Recognit. (CVPR)*, 2024, pp. 14749–14759.
- [11] Z. Li *et al.*, “BEVFormer: Learning bird’s-eye-view representation from multi-camera images via spatiotemporal transformers,” in *Proc. Eur. Conf. Comput. Vis. (ECCV)*, 2022, pp. 1–18.
- [12] J. Phillion and S. Fidler, “Lift, splat, shoot: Encoding images from arbitrary camera rigs by implicitly unprojecting to 3D,” in *Proc. Eur. Conf. Comput. Vis. (ECCV)*, 2020, pp. 194–210.
- [13] S. Wang, Y. Liu, T. Wang, Y. Li, and X. Zhang, “Exploring object-centric temporal modeling for efficient multi-view 3D object detection,” in *Proc. IEEE/CVF Int. Conf. Comput. Vis. (ICCV)*, 2023, pp. 3621–3631.
- [14] Y. Liu, T. Wang, X. Zhang, and J. Sun, “PETR: Position embedding transformation for multi-view 3D object detection,” in *Proc. Eur. Conf. Comput. Vis. (ECCV)*, 2022, pp. 531–548.
- [15] J. Huang, G. Huang, Z. Zhu, Y. Ye, and D. Du, “BEVDet: High-performance multi-camera 3D object detection in bird-eye-view,” *arXiv preprint arXiv:2112.11790*, 2021.
- [16] Y. Li *et al.*, “BEVDepth: Acquisition of reliable depth for multi-view 3D object detection,” in *Proc. AAAI Conf. Artif. Intell.*, 2023, pp. 1477–1485.
- [17] A. Kendall and Y. Gal, “What uncertainties do we need in Bayesian deep learning for computer vision?,” in *Proc. Adv. Neural Inf. Process. Syst. (NeurIPS)*, 2017, pp. 5574–5584.
- [18] B. Lakshminarayanan, A. Pritzel, and C. Blundell, “Simple and scalable predictive uncertainty estimation using deep ensembles,” in *Proc. Adv. Neural Inf. Process. Syst. (NeurIPS)*, 2017, pp. 6402–6413.
- [19] G. P. Meyer and N. Thakurdesai, “Learning an uncertainty-aware object detector for autonomous driving,” in *Proc. IEEE/RSJ Int. Conf. Intell. Robots Syst. (IROS)*, 2020, pp. 10521–10527.
- [20] Z. Song *et al.*, “Robustness-aware 3D object detection in autonomous driving: A review and outlook,” *IEEE Transactions on Intelligent Transportation Systems*, vol. 25, no. 11, pp. 15407–15436, 2024, doi: 10.1109/TITS.2024.3439557.
- [21] C. Zhang, H. Wang, Y. Cai, L. Chen, and Y. Li, “TransFusion: Multi-modal robust fusion for 3D object detection in foggy weather based on spatial vision transformer,” *IEEE Transactions on Intelligent Transportation Systems*, vol. 25, no. 9, pp. 10652–10666, 2024, doi: 10.1109/TITS.2024.3420432.
- [22] W. Wu, X. Deng, P. Jiang, S. Wan, and Y. Guo, “CrossFuser: Multi-modal feature fusion for end-to-end autonomous driving under unseen weather conditions,” *IEEE Transactions on Intelligent Transportation Systems*, vol. 24, no. 12, pp. 14378–14392, 2023, doi: 10.1109/TITS.2023.3307589.
- [23] Z. Gu *et al.*, “Belief state separated reinforcement learning for autonomous vehicle decision making under uncertainty,” in *Proc. IEEE Intell. Transp. Syst. Conf. (ITSC)*, 2021, pp. 1–6.
- [24] R. Valiente, M. Razzaghpour, B. Toghi, G. Shah, and Y. P. Fallah, “Prediction-aware and reinforcement learning-based altruistic cooperative driving,” *IEEE Transactions on Intelligent Transportation Systems*, vol. 25, no. 3, pp. 2450–2465, 2024.
- [25] K. He, X. Zhang, S. Ren, and J. Sun, “Deep residual learning for image recognition,” in *Proc. IEEE Conf. Comput. Vis. Pattern Recognit. (CVPR)*, 2016, pp. 770–778.
- [26] X. Zhu, W. Su, L. Lu, B. Li, X. Wang, and J. Dai, “Deformable DETR: Deformable transformers for end-to-end object detection,” in *Proc. Int. Conf. Learn. Represent. (ICLR)*, 2021.
- [27] I. Loshchilov and F. Hutter, “Decoupled weight decay regularization,” in *Proc. Int. Conf. Learn. Represent. (ICLR)*, 2019.
- [28] Q. Wang, B. Wu, P. Zhu, P. Li, W. Zuo, and Q. Hu, “ECA-Net: Efficient channel attention for deep convolutional neural networks,” in *Proc. IEEE/CVF Conf. Comput. Vis. Pattern Recognit. (CVPR)*, 2020, pp. 11531–11539.
- [29] J. Gu *et al.*, “ViP3D: End-to-end visual trajectory prediction via 3D agent queries,” in *Proc. IEEE/CVF Conf. Comput. Vis. Pattern Recognit. (CVPR)*, 2023, pp. 5496–5506.
- [30] Z. Zhou, J. Wang, Y.-H. Li, and Y.-K. Huang, “Query-centric trajectory prediction,” in *Proc. IEEE/CVF Conf. Comput. Vis. Pattern Recognit. (CVPR)*, 2023, pp. 17863–17872.
- [31] B. Pan, J. Sun, H. Y. T. Leung, A. Andonian, and B. Zhou, “Cross-view semantic segmentation for sensing surroundings,” *IEEE Robot. Autom. Lett.*, vol. 5, no. 2, pp. 1872–1879, 2020.
- [32] A. W. Harley, Z. Fang, J. Li, R. Ambrus, and K. Fragkiadaki, “Simple-BEV: What really matters for multi-sensor BEV perception?” in *Proc. IEEE Int. Conf. Robot. Autom. (ICRA)*, 2023, pp. 2759–2765.
- [33] Z. Zeng, Y. Yin, Z. Yuan, A. Dey, and X. Bao, “RESAR-BEV: An explainable progressive residual autoregressive approach for camera-radar fusion in BEV segmentation,” *arXiv preprint arXiv:2505.06515*, 2025.
- [34] A. Dey, Y. Yin, Z. Yuan, Z. Zeng, X. Bao, and M. M. Islam, “Enhanced BEV scene segmentation: De-noise channel attention for resource-constrained environments,” *Computers, Materials & Continua*, vol. 81, no. 1, pp. 1123–1140, 2025, doi: 10.32604/cmc.2025.074122.